# Spin-orbit coupling in $d^2$ ordered double perovskites

Gang Chen

*Department of Physics, University of Colorado, Boulder, Colorado 80309, USA and*
*JILA, University of Colorado, Boulder, Colorado 80309, USA*

Leon Balents

*Department of Physics, University of California, Santa Barbara, California 93106, USA and*
*Kavli Institute for Theoretical Physics, University of California, Santa Barbara, California 93106, USA*

We construct and analyze a microscopic model for insulating rock-salt ordered double perovskites, with the chemical formula $A_2BB'O_6$, where the magnetic ion $B'$ has a $4d^2$ or $5d^2$ electronic configuration and forms a face-centered cubic lattice. For these $B'$ ions, the combination of the triply degenerate antisymmetric two-electron orbital states and strong spin-orbit coupling forms local quintuplets with an effective spin moment $j = 2$. Moreover, due to strongly orbital-dependent exchange, the effective spins have substantial biquadratic and bicubic interactions (fourth and sixth order in the spins, respectively). This leads, at the mean-field level, to a rich ground-state phase diagram, which includes seven different phases: a uniform ferromagnetic phase with an ordering wave vector $\mathbf{p} = \mathbf{0}$ and uniform magnetization along the [111] direction, four two-sublattice phases with an ordering wave vector $\mathbf{p} = 2\pi(001)$, and two four-sublattice antiferromagnetic phases. Among the two-sublattice phases, there is a quadrupolar ordered phase that preserves time-reversal symmetry. By extending the mean-field theory to finite temperatures, we find 10 different magnetization processes with different magnetic thermal transitions. In particular, we find that thermal fluctuations stabilize the two-sublattice quadrupolar ordered phase in a large portion of the phase diagram. Existing and possible future experiments are discussed in light of these theoretical predictions.

## I. INTRODUCTION

The combination of strong electron correlation and strong spin-orbit coupling (SOC) is relatively unexplored theoretically. It arises naturally in a broad family of magnetic Mott insulating systems in which the threefold-degenerate $t_{2g}$ orbitals are partially filled. In these systems, the $t_{2g}$ orbital degeneracy is protected by cubic lattice symmetry and the crystal-field splitting is large enough so that $e_g$ orbitals are not occupied. Unlike for $e_g$ states, SOC is unquenched for $t_{2g}$ orbitals and splits the one-electron levels into an upper $j = 1/2$ doublet and a lower $j = 3/2$ quadruplet.[1,2]

In this category, many Ir-based magnets have been studied both theoretically and experimentally.[1–8] Here, the magnetic ion $Ir^{4+}$ has a $d^5$ electron configuration with five electrons residing on the $t_{2g}$ orbitals, and the effective $j = 1/2$ description can be adopted. Some very exotic states such as a quantum spin liquid in $Na_4Ir_3O_8$ (Refs. 1 and 3) and a topological Mott insulator in $A_2Ir_2O_7$ (Refs. 4 and 6–8) have been observed and proposed in the strong-coupling and intermediate-coupling regimes, respectively.

Moving beyond iridates, in our recent work,[9] we have studied the magnetic properties of a series of compounds called ordered double perovskites with the chemical formula $A_2BB'O_6$.[10–16] We considered double perovskites in which the magnetic ions $B'$ (e.g., $Re^{6+}$, $Os^{7+}$, $Mo^{5+}$) have a $d^1$ electron configuration with one electron residing on the $t_{2g}$ orbitals and, hence, form $j = 3/2$ local moments. In this analysis, we found several exotic phases including a novel ferromagnetic state driven primarily by orbital interaction, an antiferromagnetic state with strong octupolar order, a spin nematic state, and,

furthermore, a quantum spin-liquid state postulated in a region of the phase diagram.

To round out the list of magnetic systems with partially filled $t_{2g}$ orbitals, we must consider the $d^2$, $d^3$, and $d^4$ cases. For a $d^3$ electron configuration, the three electrons fill all the three single-electron $t_{2g}$ orbitals, forming an antisymmetric orbital wave function. The orbital degree of freedom is completely quenched. The system is described by spin-only Hamiltonian with spin $S = 3/2$. Since it has a large spin, one may expect it to behave rather classically.[17] For a $d^4$ electron configuration, when the SOC dominates over the Hund's coupling, the four electrons completely fill the lower $j = 3/2$ quadruplets and there is no local moment description at lowest order of approximation. When the Hund's coupling dominates over SOC, the four $t_{2g}$ electrons form a total spin $S = 1$, but still have a threefold orbital degeneracy. The effective SOC further lifts the spin-orbital degeneracy completely and also favors a trivial $j = 0$ local state. So, the only nontrivial case left is the $d^2$ configuration, with two electrons filling the $t_{2g}$ orbitals.

In this paper, we consider this valence state in the context of double perovskites mentioned above, specifically extending the theory of Ref. 9 to the case of a $B'$ ion with a $4d^2$ or $5d^2$ electron configuration.[13,18] Unlike for the $4d^1$ or $5d^1$ system with one electron per site, the local Coulomb interaction plays an important role in determining the local spin and orbital structures for the $4d^2$ or $5d^2$ systems. For the spin sector, the first Hund's rule requires a symmetrized spin wave function, favoring a *total spin $S = 1$*. For the orbital sector, the orbital electron wave function should be antisymmetrized, composed of two single-electron $t_{2g}$ orbitals. These three antisymmetrized two-electron states act as an

effective $l = 1$ *total orbital angular moment*. The strong SOC combines the total spin $S = 1$ with the total orbital moment $l = 1$ and leads to an effective total angular momentum $j = 2$ description of the system. Similar to the $j = 3/2$ case studied in Ref. 9, the orbitally dependent nature of the spin interactions leads to an interesting microscopic Hamiltonian, which contains significant biquadratic (fourth order in spin operators) and triquadratic (sixth order in spin operators) spin-spin interactions. These unusual interactions may be understood as couplings between the local magnetic quadrupole and octupole moments. Therefore, an analysis of the microscopic Hamiltonian naturally leads to a rich structure of magnetic multipolar orders.

The results of a mean-field analysis are summarized in Fig. 1 and Table I. There are seven total ground-state phases that appear, including notably a broad region of time-reversal invariant but quadrupolar ordered (spin nematic) ground state with a two-sublattice structure of the orbital configuration. This is described by the quadrupole tensor operators

$$Q_i^{3z^2} = \left[ 2\left(j_i^z\right)^2 - \left(j_i^x\right)^2 - \left(j_i^y\right)^2 \right]/\sqrt{3}, \qquad (1)$$

$$Q_i^{x^2-y^2} = \left(j_i^x\right)^2 - \left(j_i^y\right)^2. \qquad (2)$$

In the quadrupolar phase, $\langle Q_i^{x^2-y^2} \rangle = \pm q'$ alternates sign on the two sublattices [see Eqs. (73)]. In this phase, the time-reversal symmetry is *unbroken* and there is no magnetic dipolar and octupolar order. Such a *local* spin nematic ground state is particular to integer spin systems and prohibited for half-integer spins. A similar spin nematic ground state has also been proposed theoretically for a spin $S = 1$ material NiGa$_2$S$_4$,[19–24] but an experimental confirmation of this phase in NiGa$_2$S$_4$ is still lacking. Apart from the quadrupolar ordered phase, the other ground states are magnetic and comprise both ferromagnetic and antiferromagnetic states with enlarged unit cells up to quadruple the size of the ideal one. The extension of the mean-field analysis to $T > 0$ is described in Fig. 2. Amongst various finite-temperature phases, the quadrupolar ordered one is prominent, providing more opportunity for its experimental discovery in real material.
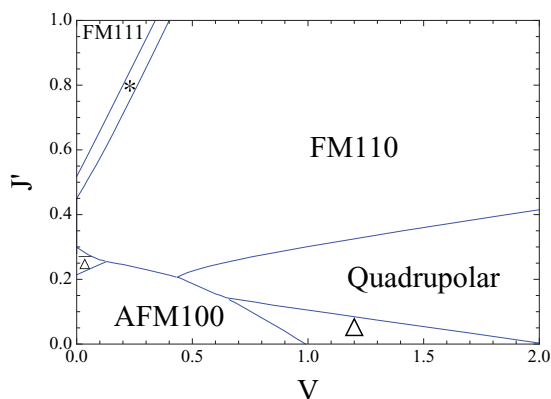
TABLE I. Phases in mean-field theory. The first column gives the name of the phase, as shown in Fig. 1. In the second column, $\vec{m}$ denotes the direction (up to symmetries) of the uniform magnetization; a "0" is shown if this is vanishing. Similarly, in the third column, $\vec{n}$ denotes the direction of the staggered magnetization. For the quadrupolar phase, in which "0" appears in both the second and third columns, time-reversal symmetry is unbroken. The fourth column specifies the number of sites in the magnetic unit cell. The fifth column gives the number of sites in the unit cell for time-reversal-invariant observables, i.e., the quadrupolar tensor.

| Phase | $\vec{m}$ | $\vec{n}$ | Magnetic unit cell | Quadrupolar unit cell |
|---|---|---|---|---|
| AFM100 | 0 | [100] | 2 | 1 |
| FM111 | [111] | 0 | 1 | 1 |
| FM110 | [110] | [1$\bar{1}$0] | 2 | 2 |
| | [11x] | [1$\bar{1}$0] | 2 | 2 |
| $\Delta$ | 0 | [xy0] | 4 | 2 |
| $\overline{\Delta}$ | 0 | [xy0] | 4 | 1 |
| Quadrupolar | 0 | 0 | 2 | 2 |

The remainder of the paper is organized as follows. In Sec. II, we first explain the on-site spin and orbital physics, which leads to effective $j = 2$ local moments on each $B'$ magnetic ion. As we did in previous work,[9] we introduce a microscopic Hamiltonian, which includes three interactions: nearest-neighbor (NN) antiferromagnetic (AFM) exchange $J$, NN ferromagnetic (FM) exchange $J'$, and electric quadrupolar interaction $V$. Due to strong SOC, we project these interactions, which are written in the separate spin and orbital spaces, down to the $j = 2$ manifold. This leads to a spatially anisotropic and very non-Heisenberg-type Hamiltonian, which contains many terms beyond the usual quadratic exchange. In Sec. III, we find the mean-field ground-state phase diagram
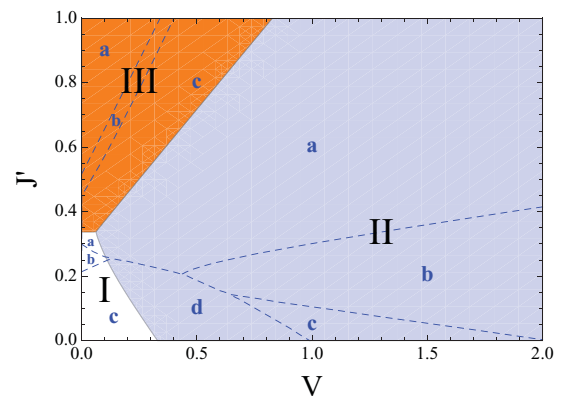


FIG. 2. (Color online) $T > 0$ phase diagram. In region I (white), the system transitions directly from the high-temperature paramagnetic phase to a magnetic state with ordering wave vector $\mathbf{Q} = 2\pi(001)$ at $T = T_m(\mathbf{Q})$. In region II (blue), the transition from the high-temperature paramagnet is instead to a quadrupolar phase with ordering wave vector $\mathbf{Q}$ at $T = T_Q(\mathbf{Q})$. In region III (red), the transition from the paramagnetic is to a $\mathbf{q} = \mathbf{0}$ ferromagnetic state at $T = T_m(\mathbf{0})$. The dashed curves are the boundaries of the ground-state phases taken from Fig. 1. a, b, c, and d label the low-temperature phases of each region. $J = 1$ in the phase diagram.



FIG. 1. (Color online) Ground-state phase diagram of the model Hamiltonian in Eq. (24). Here, $V$ is the electric quadrupole interaction, and $J'$ is the nearest-neighbor ferromagnetic exchange between orthogonal orbitals; both are normalized to a unit value $J = 1$ for the nearest-neighbor antiferromagnetic coupling. The names for the phases are defined in Table I, and in Sec. III.

of the model Hamiltonian and analyze the properties of each ground state. Some insight into the general results is given by considering some simple limits, including both strong easy plane and easy axis anisotropy, and an orbital interaction only model (Sec. III B). We find that, aside from a uniform orbitally ordered, there exists an orbitally ordered state with a two sublattice structure. Finally, in Sec. III C, we carry out a mean-field study for the complete model Hamiltonian and find the zero-temperature ground-state phase diagram, which is depicted in Fig. 1.

In Sec. IV, we extend the mean-field theory to $T > 0$, and identify the structure of the magnetic order for each phase. We find 10 different finite-temperature magnetization processes, which correspond to the 10 overlapping regions between the ground-state phases and the shaded areas in Fig. 2. We also discuss the different finite-temperature phase transitions associated with magnetic dipolar and quadrupolar orders. Transition temperatures are extracted from Landau theory. In a broad region of the parameter space, we find that the quadrupolar phase occurs at the intermediate temperatures between the high-temperature paramagnetic phase and various low-temperature magnetic ordered phases. Finally, in Sec. V, we compare our theoretical predictions with current experimental findings and suggest further directions for theory and experiment.

## II. MODEL

### A. Spin-orbit interaction and electron orbitals

The magnetic ions $B'$ ($Re^{5+}$, $Os^{6+}$) in the relevant ordered double perovskites ($Ba_2CaOsO_6$, $La_2LiReO_6$, $Ba_2YReO_6$)[13,18] all have a $4d^2$ or $5d^2$ electron configuration with two electrons on the triply degenerate $t_{2g}$ multiplets. Because of the electron interaction, the local spin-orbital state is quite different from the case of $d^1$ electron configuration where the single-electron state is enough to describe the local physics. Considering the dominance of the crystal-field splitting over the SOC, we now fill the three $t_{2g}$ orbitals with these two electrons before including the effect of SOC. To respect the first Hund's rule, the total spin for the two electrons is $S = 1$. For the orbital sector, there are three degenerate antisymmetric two-electron states:

$$|X\rangle = \frac{1}{\sqrt{2}}(|xy\rangle_1|xz\rangle_2 - |xy\rangle_2|xz\rangle_1), \tag{3}$$

$$|Y\rangle = \frac{1}{\sqrt{2}}(|xy\rangle_1|yz\rangle_2 - |xy\rangle_2|yz\rangle_1), \tag{4}$$

$$|Z\rangle = \frac{1}{\sqrt{2}}(|xz\rangle_1|yz\rangle_2 - |xz\rangle_2|yz\rangle_1), \tag{5}$$

in which the subindices ("1" and "2") label the electron. Therefore, there are totally ninefold spin-orbital degeneracies. The presence of SOC will lift some of the degeneracies. Following the spirit of degenerate perturbation theory, we project the SOC onto the triplet subspace spanned Eq. (5):

$$\mathcal{H}_{\text{so}} = -\lambda\,\mathbf{l}\cdot\mathbf{S}\,, \tag{6}$$

in which the total angular momentum quantum numbers of these operators are $l = 1, S = 1$. The effective orbital angular

momentum $\mathbf{l}$ comes from the projection of the *total* orbital angular momentum $\mathbf{L} \equiv \mathbf{L}_1 + \mathbf{L}_2$ onto the tripets in Eq. (5),

$$\mathcal{P}_o\,\mathbf{L}\,\mathcal{P}_o = -\mathbf{l}\,. \tag{7}$$

Here, $\mathcal{P}_o \equiv \sum_{A=X,Y,Z} |A\rangle\langle A|$ is the projection operator to the triplet orbital subspace. The reduced SOC in Eq. (6) favors a local $j = 2$ ($\mathbf{j} = \mathbf{l} + \mathbf{S}$) over other higher-energy states $j = 0, 1$ by an energy separation $O(\lambda)$. In the materials we are considering, the SOC $\lambda$ is a very large energy scale (some fraction of an eV).

In general, cubic symmetry allows the presence of an onsite cubic anisotropy term $(j^x)^4 + (j^y)^4 + (j^z)^4$, which lifts the degeneracy of the five $j = 2$ states. However, we expect this splitting to be rather small, and provided it is smaller than the typical exchange coupling between spins, the $j = 2$ description should be a good approximation. Microscopically, the cubic anisotropy comes from the fourth-order effect of the SOC and pair hopping (between different orbitals on the same ion) terms $J_p$, which excite the electrons into the $e_g$ orbitals. The magnitude of the cubic anisotropy should be of $\sim O(\lambda^4/\Delta^3, J_p^4/\Delta^3)$ (with $\Delta$ the crystal-field splitting between $e_g$ and $t_{2g}$ levels). This is certainly a much smaller energy scale compared to SOC, and likely small compared to exchange. In any case, we will neglect it in the following.

In the strong SOC limit, every local operator should be projected onto the local subspace spanned by five $j = 2$ states. In particular,

$$\mathcal{P}_2\,\mathbf{S}\,\mathcal{P}_2 = \tfrac{1}{2}\mathbf{j}, \tag{8}$$

$$\mathcal{P}_2\,\mathbf{l}\,\mathcal{P}_2 = \tfrac{1}{2}\mathbf{j}\,. \tag{9}$$

Here, $\mathcal{P}_2$ is the projection operator into the local $j = 2$ states. In addition, one can find that the local magnetic moment is given by

$$\mathbf{M} = \mathcal{P}_2\,(2\mathbf{S} - \mathbf{l})\,\mathcal{P}_2 = \tfrac{1}{2}\mathbf{j}\,, \tag{10}$$

hence, the magnitude of the local magnetic moment is found to be $\sqrt{6}/2\mu_{\text{B}} \approx 1.25\mu_{\text{B}}$.

### B. Exchange interactions and electric quadrupolar interaction

In this section, we introduce the interactions between the local moments. From previous work,[9] we will need to consider the nearest-neighbor antiferromagnetic exchange, NN FM exchange, and NN electric quadrupolar interactions, and these interactions are highly anisotropic in both the position and spin spaces. For example, in the $XY$ plane, only electrons on $xy$ orbital can virtually transfer from one site to another via the intermediate oxygen $p$ orbitals. Thus, one finds that the NN AFM exchange is written as

$$\mathcal{H}_{\text{AFM}}^{XY} = J \sum_{\langle ij\rangle \in XY} \left[ \mathbf{S}_{i,xy}\cdot\mathbf{S}_{j,xy} - \frac{1}{4}n_{i,xy}n_{j,xy} \right], \tag{11}$$

where the sum is over nearest-neighbor sites in the $XY$ planes, and the correponding terms for the $YZ$ and $XZ$ planes can be obtained by the obvious cubic permutation. One should note that the operators $\mathbf{S}_{i,xy}$ and $n_{i,xy}$ denote the electron spin residing on the single-electron $xy$ orbital and orbital occupation number for the single-electron $xy$ orbital at site $i$, respectively. To connect these single-electron operators to the

two-electron operator, which acts on the two-electron orbitals in Eq. (5), we have the following relations:

$$n_{i,xy} = n_{i,X} + n_{i,Y} = \left(l_i^z\right)^2, \tag{12}$$

$$\mathbf{S}_{i,xy} = \frac{\mathbf{S}_i}{2}(n_{i,X} + n_{i,Y}) = \frac{\mathbf{S}_i}{2}\left(l_i^z\right)^2. \tag{13}$$

Here, $n_{i,X}$ (or $n_{i,Y}$) denotes the occupation number for $|X\rangle$ (or $|Y\rangle$) of the two-electron orbital states at site $i$, and $\mathbf{S}_i$ is the total spin $S = 1$ for the two electrons. The physical meaning of Eq. (13) is apparent. The electron occupation number on the single-electron orbital $xy$ can be nonvanishing only when the two-electron orbital state $|X\rangle$ or $|Y\rangle$ is occupied by the two electrons.

Throughout this paper, we use the subindices $(i,xy)$ to denote the site and single-electron orbitals, subindex X to denote the two-electron orbitals, superindex $(\mu = x,y,z)$ to denote the spin component, and capital letters ($XY$, $XZ$, $YZ$) to denote the planes. With these definitions, we note that the double-occupancy condition at each site, which defines the Mott insulating phase, becomes

$$n_{i,xy} + n_{i,xz} + n_{i,yz} = 2 \tag{14}$$

in terms of the two-electron operators, the above equation is equivalent to

$$n_{i,X} + n_{i,Y} + n_{i,Z} = 1. \tag{15}$$

Moreover, from Eq. (13), orbitally resolved spins satisfy

$$\mathbf{S}_{i,xy} + \mathbf{S}_{i,xz} + \mathbf{S}_{i,yz} = \mathbf{S}_i. \tag{16}$$

The second interaction to include is the NN FM exchange interaction. FM exchange comes about when the orthogonal $p$ orbitals on a single oxygen ion are involved in the exchange path. Directly using the results from Ref. 9 and the relation in Eq. (13), one can immediately write down this interaction. Again, for two sites $i,j$ in the $XY$ plane, this FM exchange is given as

$$\begin{aligned} \mathcal{H}_{\mathrm{FM},ij}^{XY} &= -J'[\mathbf{S}_{i,xy} \cdot (\mathbf{S}_{j,yz} + \mathbf{S}_{j,xz}) + \langle i \leftrightarrow j \rangle] + \frac{3J'}{2}n_{i,xy}n_{j,xy} \\ &= -\frac{J'}{4}\left\{\mathbf{S}_i \cdot \mathbf{S}_j\left(l_i^z\right)^2\left[\left(l_j^x\right)^2 + \left(l_j^y\right)^2\right] + \langle i \leftrightarrow j \rangle\right\} \\ &\quad + \frac{3J'}{4}\left(l_i^z\right)^2\left(l_j^z\right)^2. \end{aligned} \tag{17}$$

The third interaction to include is the electric quadrupolar interaction. This is obtained by evaluating the Coulomb interaction in different orbital occupations. As the AFM and FM exchange, we also take results from previous work to write down this interaction. In the $XY$ plane, we obtain the electric quadrupolar interaction as

$$\begin{aligned} \mathcal{H}_{\mathrm{quad},ij}^{XY} &= -\frac{4V}{3}(n_{i,xz} - n_{i,yz})(n_{j,xz} - n_{j,yz}) + \frac{9V}{4}n_{i,xy}n_{j,xy} \\ &= -\frac{4V}{3}\left[\left(l_i^y\right)^2 - \left(l_i^x\right)^2\right]\left[\left(l_j^y\right)^2 - \left(l_j^x\right)^2\right] \\ &\quad + \frac{9V}{4}\left(l_i^z\right)^2\left(l_j^z\right)^2. \end{aligned} \tag{18}$$

The minimal Hamiltonian for the cubic system contains all three of these interactions in addition to the on-site SOC:

$$\mathcal{H} = \mathcal{H}_{\mathrm{AFM}} + \mathcal{H}_{\mathrm{FM}} + \mathcal{H}_{\mathrm{quad}} + \mathcal{H}_{\mathrm{so}}. \tag{19}$$

Since we are interested in the limit of strong SOC, we have to project the minimal Hamiltonian $\mathcal{H}$ onto the five $j = 2$ states at every site. As an illustration, we write down the projection for $\mathbf{S}_{i,xy}$ and $n_{i,xy}$ as

$$\tilde{S}_{i,xy}^x = \frac{1}{12}j_i^x + \frac{1}{12}\left(j_i^x\right)^3, \tag{20}$$

$$\tilde{S}_{i,xy}^y = \frac{1}{12}j_i^x + \frac{1}{12}\left(j_i^x\right)^3, \tag{21}$$

$$\tilde{S}_{i,xy}^z = -\frac{1}{12}j_i^x + \frac{1}{12}\left(j_i^x\right)^3, \tag{22}$$

$$\tilde{n}_{i,xy} = \frac{1}{3} + \frac{1}{6}\left(j_i^z\right)^2, \tag{23}$$

in which $\tilde{O} = \mathcal{P}_2 O \mathcal{P}_2$. After the projection, the minimal Hamiltonian that we will study in this paper is

$$\tilde{\mathcal{H}} = \tilde{\mathcal{H}}_{\mathrm{AFM}} + \tilde{\mathcal{H}}_{\mathrm{FM}} + \tilde{\mathcal{H}}_{\mathrm{quad}}. \tag{24}$$

## III. MEAN-FIELD GROUND STATES

In this section, we study the zero-temperature phase diagram of the model Hamiltonian in Eq. (24). Ultimately, in Sec. III C, we will do this by mean-field theory, or equivalently, variationally searching for direct product states that minimize the expectation of $\tilde{\mathcal{H}}$. Before reporting these results, however, we discuss some simple limits in which the behavior can be understood more intuitively. First, in Sec. III A, we impose a strong single-ion uniaxial anisotropy, which removes the orbital degeneracy and renders the problem trivially soluble with singlet, ferromagnetic, and antiferromagnetic ground states. Second, we consider a pure orbital model in which only the electric quadrupole interaction $V$ is included. This gives the two-sublattice quadrupolar state described in the Introduction. Finally, in Sec. III C, we report the results of a full mean-field calculation including all couplings and making no further approximations.

### A. Uniaxial anisotropy

As we did in Ref. 9, we first consider the ground state of this Hamiltonian in the presence of strong easy-plane or easy-axis anisotropies. The strong easy-plane anisotropy (on the $XY$ plane) is a trivial limit and is modeled by $\sum_i D(j_i^z)^2$ with a positive $D$. When $D$ is quite large (compared to exchange coupling and electric quadrupolar interaction), the spin state on every site is pinned to $|j^z = 0\rangle$, which is a rather trivial uniform state with an ordering wave vector $\mathbf{p} = 0$. The strong easy-axis anisotropy (along the $z$ direction) is less trivial and is modeled by the same Hamiltonian but with a negative $D$. Large $|D|$ favors either $|j^z = 2\rangle$ or $|j^z = -2\rangle$ to be occupied. After projecting the Hamiltonian in Eq. (24) onto these two states, the electric quadrupolar interaction is completely quenched and the resulting effective Hamiltonian is a trivial Ising Hamiltonian. One can readily find that, when $J' \geqslant 5J/38$, the ground state is a ferromagnetic state with an ordering wave vector $\mathbf{p} = \mathbf{0}$, and when $J' \leqslant 5J/38$, the ground state is an antiferromagnetic state with an ordering wave vector $\mathbf{p} = 2\pi(100)$ or $2\pi(010)$. One may postulate from

these anisotropic cases that the ground state for the actual cubic Hamiltonian may either have a uniform state ($\mathbf{p} = \mathbf{0}$) or a two-sublattice state [$\mathbf{p} = 2\pi(001)$ and equivalent wave vectors]. As we will see in the following sections, this guess is correct for a large portion of the parameter space, but we also find some interesting exceptions.

### B. Orbital Hamiltonian

To understand the nature of the nonmagnetic quadrupolar ground state of the model, it is sufficient to consider only the electric quadrupole interaction $V$, given in Eq. (18). Note that it involves only the three operators $\tilde{n}_{i,yz}$, $\tilde{n}_{i,xz}$, and $\tilde{n}_{i,xy}$ on each site. Since these are all time-reversal invariant, it is apparent that they do not span the full space of $j = 2$ operators. Thus, there must be additional constants of the motion, and the Hamiltonian can be separated into sectors corresponding to different irreducible representations (irreps) of the algebra of these operators. Indeed, one can show that the single-site Hilbert space decomposes into one two-dimensional irrep and three one-dimensional irreps. The two-dimensional irrep is spanned by the two states

$$|u\rangle = \frac{1}{\sqrt{2}}(|j^z = 2\rangle + |j^z = -2\rangle), \quad (25)$$

$$|d\rangle = |j^z = 0\rangle. \quad (26)$$

In this subspace, the orbital operators become

$$\tilde{n}_{i,yz} = \frac{2}{3} - \frac{1}{6}\sigma_i^z + \frac{1}{2\sqrt{3}}\sigma_i^x, \quad (27)$$

$$\tilde{n}_{i,xz} = \frac{2}{3} - \frac{1}{6}\sigma_i^z - \frac{1}{2\sqrt{3}}\sigma_i^x, \quad (28)$$

$$\tilde{n}_{i,xy} = \frac{2}{3} + \frac{1}{3}\sigma_i^z, \quad (29)$$

where $\vec{\sigma}_i$ are the Pauli matrices acting in the $|u\rangle, |d\rangle$ space. In the first of the three one-dimensional irreps, we have

$$\begin{pmatrix} \tilde{n}_{i,yz} \\ \tilde{n}_{i,xz} \\ \tilde{n}_{i,xy} \end{pmatrix} = \begin{pmatrix} 1/2 \\ 1/2 \\ 1 \end{pmatrix}. \quad (30)$$

The other two one-dimensional irreps may be obtained by permuting these values.

The ground state must consist of a single irrep on each site. Which irrep occurs should be determined by minimization of the energy. Consider the case in which each site has a one-dimensional irrep. Then, we can specify the state of a site by a "Potts"-type variable $s_i = 1,2,3$ specifying which of the three orbital numbers equals 1, i.e.,

$$\tilde{n}_{i,a} = \tfrac{1}{2} + \tfrac{1}{2}\delta_{s_i,a}, \quad (31)$$

with $a = 1,2,3$ corresponding to $a = yz, xz, xy$, respectively. Then, the Hamiltonian for a bond in the $XY$ plane becomes

$$\tilde{\mathcal{H}}_{ij}^{XY}\big|_{\text{1d irreps}} = -\frac{V}{3}(\delta_{s_i,1} - \delta_{s_i,2})(\delta_{s_j,1} - \delta_{s_j,2}) + \frac{9V}{16}(1 + \delta_{s_i,3})(1 + \delta_{s_j,3}), \quad (32)$$

with $YZ$ and $XZ$ plane bond interactions obtained by permutations. In this case, the Hamiltonian is purely classical and thus

the ground state can be exactly found by minimization. We find that a ferromagnetic ground state is preferred, with constant $s_i$ (there are thus three such degenerate ground states), which has an average energy of $65V/72 \approx 0.903V$ per bond.

The other natural choice to consider is when the two-dimensional irrep is chosen on each site. In this case, the Hamiltonian can be written as

$$\tilde{\mathcal{H}}_{ij}^{XY}\big|_{\text{2d irrep}} = V\big[1 - \tfrac{25}{36}\sigma_i^x\sigma_j^x + \tfrac{1}{4}\vec{\sigma}_i \cdot \vec{\sigma}_j\big], \quad (33)$$

where the dot product involves only the $x$ and $z$ components of the Pauli matrices, and we have dropped a term linear in the Pauli matrices, which cancels when all three types of bonds are added. In this case, the interactions for bonds in the other two planes are obtained by the rotations $\sigma_i^x \to -\frac{1}{2}\sigma_i^x \pm \frac{\sqrt{3}}{2}\sigma_i^z$, with the upper (lower) sign chosen for the $XZ$ ($YZ$) plane. The dot product is unchanged by this rotation.

The Hamiltonian in this subspace is a type of Kugel-Khomskii model, similar to that studied in models of $e_g$ orbitals. It is fully quantum and, thus, can not be solved exactly. However, within mean-field theory, we find that the variational ground state is simply the antiferromagnetic product state with $\sigma_i^x = (-1)^z$, i.e., with alternating sign on adjacent $XY$ planes. In this state, the expectation of the Hamiltonian can be taken, and the energy is found to be $E_v = 173V/216 \approx 0.801V$ per bond. Note that this is lower than the energy found for the one-dimensional irreps. This is an upper (variational) bound on the ground-state energy in this sector, so we indeed expect the ground state to be in the two-dimensional irrep.

Physically, the mean-field state describes an orbitally ordered phase with a two-sublattice structure with single-ion wave functions

$$|A\rangle = \frac{1}{2}|j^z = 2\rangle + \frac{1}{\sqrt{2}}|j^z = 0\rangle + \frac{1}{2}|j^z = -2\rangle, \quad (34)$$

$$|B\rangle = \frac{1}{2}|j^z = 2\rangle - \frac{1}{\sqrt{2}}|j^z = 0\rangle + \frac{1}{2}|j^z = -2\rangle, \quad (35)$$

where $A$, $B$ label the two different sublattices (planes with even and odd $z$). Remarkably, these states are *invariant* under time reversal. Since time-reversal symmetry is unbroken, there is no magnetic order

$$\langle \mathbf{j}_i \rangle = 0. \quad (36)$$

Therefore, this phase is a magnetic quadrupolar phase (or spin nematic phase) and the orbital configuration is given by

$$\langle \tilde{\mathbf{n}}_A \rangle = \left(\frac{2}{3} + \frac{\sqrt{3}}{6}, \frac{2}{3} - \frac{\sqrt{3}}{6}, \frac{2}{3}\right) \quad (37)$$

$$\langle \tilde{\mathbf{n}}_B \rangle = \left(\frac{2}{3} - \frac{\sqrt{3}}{6}, \frac{2}{3} + \frac{\sqrt{3}}{6}, \frac{2}{3}\right). \quad (38)$$

Here, we defined $\tilde{\mathbf{n}} \equiv (\tilde{n}_{yz}, \tilde{n}_{xz}, \tilde{n}_{xy})$ for convenience.

### C. Full cubic Hamiltonian

Although both the anisotropic limit and pure orbital interaction support a two-sublattice ground state, it is still questionable that the cubic Hamiltonian will also behave likewise. In this section, we report the results of a systematic investigation of the mean-field ground states of the full

Hamiltonian, allowing for large unit cells (we considered cells of up to four sites). We made no further assumptions and variationally minimized the energy with respect to an arbitrary wave function on every site of the unit cell. Finally, we verified that each mean-field ground state is stable within linear-flavor wave theory.[9] The mean-field phase diagram is depicted in Fig. 1, and the key features of each phase are listed in Table I. Within the flavor wave theory, all seven phases exhibit an energy gap. Next, we describe each of the seven phases.

### 1. Antiferromagnetic (AFM100) state

For small $J'/J$ and $V/J$, the ground state is a typical antiferromagnetic phase with an ordering wave vector $\mathbf{p} = 2\pi(001)$. States with the equivalent momenta $\mathbf{p} = 2\pi(100), 2\pi(010)$ are, of course, degenerate. To be specific, we will take $\mathbf{p} = 2\pi(001)$ for all the two-sublattice phases in the following. The variational mean-field ground-state wave function on the $A$ and $B$ sublattices has the following form:

$$|A\rangle = \frac{x}{\sqrt{2}}(|j^z = 2\rangle + |j^z = -2\rangle) + \sqrt{\frac{1}{2} - x^2}|j^z = 0\rangle$$
$$+ \frac{1}{2}(|j^z = 1\rangle + |j^z = -1\rangle), \qquad (39)$$

$$|B\rangle = \frac{x}{\sqrt{2}}(|j^z = 2\rangle + |j^z = -2\rangle) + \sqrt{\frac{1}{2} - x^2}|j^z = 0\rangle$$
$$- \frac{1}{2}(|j^z = 1\rangle + |j^z = -1\rangle), \qquad (40)$$

in which $x$ is a real parameter, which is found by minimizing the variational energy. Since, under time reversal, $|j^z = m\rangle \rightarrow (-1)^m|j^z = m\rangle$, these two states transform into one other under time reversal. Therefore, the magnetic dipolar and octupolar orders are antiparallel on two sublattices. Because of the intrinsic strong SOC, the local moments are aligned by crystalline anisotropy and in this state orient along the [100] (or, equivalently, [010]) axis. A more precise description of the symmetry breaking of the phase is given by introducing the magnetic dipole and quadrupole moment operators. The magnetic dipole moment is antiferromagnetically ordered,

$$\langle \mathbf{j}_{A/B} \rangle = \pm m(1,0,0), \qquad (41)$$

with $m = \sqrt{2}x + \sqrt{3(1 - 2x^2)}$. The magnetic quadrupole tensor, however, is uniformly ordered,

$$\langle Q_i^{3z^2} \rangle \equiv 2\sqrt{3}(3\langle \tilde{n}_{i,xy} \rangle - 2) = q, \qquad (42)$$

$$\langle Q_i^{x^2 - y^2} \rangle \equiv 6\langle \tilde{n}_{i,yz} - \tilde{n}_{i,xz} \rangle = q' \qquad (43)$$

with $q = 2\sqrt{3}(2x^2 - 3/4)$ and $q' = 2\sqrt{3(1 - 2x^2)} + 3/2$.

The uniform quadrupolar order (or orbital configuration) can be understood to arise from the large NN AFM exchange $J$, which favors time-reversal pairs on two sublattices. As the ferromagnetic exchange and electric quadrupolar interaction

increase, the orbital-orbital interaction will become important and the uniform orbital structure will break down.

### 2. Uniform ferromagnetic (FM111) state

With large $J'/J$ and small $V/J$, the ferromagnetic exchange dominates and favors a uniform ground state with the spin polarization aligned with [111] or other equivalent lattice directions. The mean-field ground state of this phase is a fully polarized spin eigenstate with quantization axis along [111], so that

$$\langle \mathbf{j}_i \rangle = \frac{m}{\sqrt{3}}(1,1,1) \qquad (44)$$

with $m = 2$. And, the three orbitals are equally populated,

$$\langle \tilde{\mathbf{n}}_i \rangle = \left(\frac{2}{3}, \frac{2}{3}, \frac{2}{3}\right), \qquad (45)$$

and the magnetic quadrupolar orders vanish,

$$\langle Q_i^{3z^2} \rangle = \langle Q_i^{x^2 - y^2} \rangle = 0. \qquad (46)$$

### 3. Two-sublattice ferromagnetic (FM110) state

With large $J'/J$ and $V/J$, we obtain a FM110 state, which is the same phase proposed in Ref. 9. This state can be considered as a compromise between the tendencies of $J$ and $J'$ to order the moments along the [100] and [111] axes. The competition between these two effects allows the orbital interaction to stabilize a coexisting quadrupolar order. The result is that the orbital configuration has a two-sublattice structure, and the magnetic moments on the two sublattices are neither antiparallel nor parallel. The ground-state wave function of this phase is parametrized by two complex numbers $x_1$ and $x_2$:

$$|A\rangle = \frac{1}{\sqrt{2}}(x_2|j^z = 2\rangle + \overline{x_2}|j^z = -2\rangle) + x_0|j^z = 0\rangle$$
$$+ \frac{1}{\sqrt{2}}(x_1|j^z = 1\rangle + \overline{x_1}|j^z = -1\rangle), \qquad (47)$$

$$|B\rangle = \frac{1}{\sqrt{2}}(-\overline{x_2}|j^z = 2\rangle - x_2|j^z = -2\rangle) + x_0|j^z = 0\rangle$$
$$+ \frac{1}{\sqrt{2}}(-i\overline{x_1}|j^z = 1\rangle + ix_1|j^z = -1\rangle), \qquad (48)$$

where $x_0 = \sqrt{1 - |x_1|^2 - |x_2|^2}$ and $\overline{x_{1,2}}$ is the complex conjugation of $x_{1,2}$. From the wave function, we find that magnetic dipole and quadrupole moments have the following form:

$$\langle \mathbf{j}_{A/B} \rangle = m\frac{1}{\sqrt{2}}(1,1,0) \pm m'\frac{1}{\sqrt{2}}(1, -1,0), \qquad (49)$$

$$\langle Q_{A/B}^{3z^2} \rangle = q, \qquad (50)$$

$$\langle Q_{A/B}^{x^2 - y^2} \rangle = \pm q'. \qquad (51)$$

Here, the actual expression of $m, m', q, q'$ in terms of $x_1$ and $x_2$ is quite involved and not important for the purpose of presentation. So, we will not write them out explicitly. Similar omissions are made in later sections.

From Eq. (51), the total magnetic moment is along the [110] direction, and the staggered magnetic dipole moment is perpendicular to the total magnetic dipole moment and

along the [1$\bar{1}$0] direction. The orbital configurations of the two sublattices are similar to that in the quadrupolar phase [see Eq. (38)].

#### 4. Intermediate ferromagnetic ("∗") state

Between the FM111 and FM110 phases, we find an intermediate state, which we denote "∗". This state also has a two-sublattice structure with the ordering wave vector $\mathbf{p} = 2\pi(001)$. We find that the ground-state wave function of this phase is parametrized by four complex numbers $x_1, x_2, x_{-1}$, and $x_{-2}$:

$$|A\rangle = x_2|j^z = 2\rangle + x_1|j^z = 1\rangle + x_0|j^z = 0\rangle$$
$$+ x_{-1}|j^z = -1\rangle + x_{-2}|j^z = -2\rangle, \qquad (52)$$

$$|B\rangle = -\overline{x_2}|j^z = 2\rangle - i\overline{x_1}|j^z = 1\rangle + x_0|j^z = 0\rangle$$
$$+ i\overline{x_{-1}}|j^z = -1\rangle - \overline{x_{-2}}|j^z = -2\rangle \qquad (53)$$

with $x_0 = \sqrt{1 - |x_1|^2 - |x_2|^2 - |x_{-1}|^2 - |x_{-2}|^2}$. The magnetic order in this phase interpolates between that of the FM111 and FM110 phases. The uniform magnetization orients along an axis between the [111] and [110] directions. As in the FM110 phase, the staggered magnetic dipole moment in phase "∗" is along the [1$\bar{1}$0] direction. The orbital configuration has the same two-sublattice structure as in the FM110 phase. The corresponding order parameters are

$$\langle \mathbf{j}_{A/B}\rangle = (m_1, m_1, m_2) \pm m'\frac{1}{\sqrt{2}}(1, -1, 0), \qquad (54)$$

$$\langle Q_{A/B}^{3z^2}\rangle = q, \qquad (55)$$

$$\langle Q_{A/B}^{x^2-y^2}\rangle = \pm q'. \qquad (56)$$

#### 5. Four-sublattice antiferromagnetic ("Δ") state

In the region of a small $J'/J$ and an intermediate $V/J$, the FM exchange interaction between time-reversal odd moments has negligible effect, while the AFM exchange and electric quadrupolar coupling are somewhat balanced. The keen competition between these two interactions induces an interesting intermediate phase: a four-sublattice antiferromagnetic phase, which we denote "Δ". The magnetic unit cell is the elementary tetrahedron of the face-centered cubic (fcc) lattice. Similar to the FM110 phase, the ground-state wave function is found to be parametrized by two complex numbers $x_1$ and $x_2$:

$$|A\rangle = \frac{1}{\sqrt{2}}(x_2|j^z = 2\rangle + \overline{x_2}|j^z = -2\rangle) + x_0|j^z = 0\rangle$$
$$+ \frac{1}{\sqrt{2}}(x_1|j^z = 1\rangle + \overline{x_1}|j^z = -1\rangle), \qquad (57)$$

$$|B\rangle = \frac{1}{\sqrt{2}}(x_2|j^z = 2\rangle + \overline{x_2}|j^z = -2\rangle) + x_0|j^z = 0\rangle$$
$$+ \frac{1}{\sqrt{2}}(-x_1|j^z = 1\rangle - \overline{x_1}|j^z = -1\rangle), \qquad (58)$$

$$|C\rangle = \frac{1}{\sqrt{2}}(-x_2|j^z = 2\rangle - \overline{x_2}|j^z = -2\rangle) + x_0|j^z = 0\rangle$$
$$+ \frac{1}{\sqrt{2}}(-ix_1|j^z = 1\rangle + i\overline{x_1}|j^z = -1\rangle), \qquad (59)$$

$$|D\rangle = \frac{1}{\sqrt{2}}(-x_2|j^z = 2\rangle - \overline{x_2}|j^z = -2\rangle) + x_0|j^z = 0\rangle$$
$$+ \frac{1}{\sqrt{2}}(ix_1|j^z = 1\rangle - i\overline{x_1}|j^z = -1\rangle) \qquad (60)$$

with $x_0 = \sqrt{1 - |x_1|^2 - |x_2|^2}$. The order parameters are

$$\langle \mathbf{j}_{A/B}\rangle = \pm m(u_1, u_2, 0), \qquad (61)$$

$$\langle \mathbf{j}_{C/D}\rangle = \pm m(-u_2, u_1, 0), \qquad (62)$$

$$\langle Q_{A/B/C/D}^{3z^2}\rangle = q, \qquad (63)$$

$$\langle Q_{A/B}^{x^2-y^2}\rangle = \langle Q_{C/D}^{x^2-y^2}\rangle = \pm q'. \qquad (64)$$

It is easy to see from the above order parameters that the orbital configuration still has a two-sublattice structure as demanded by the orbital-orbital interaction, while the magnetic dipolar order has a four-sublattice antiferromagnetic structure. One can think of this state as breaking time-reversal symmetry on top of a two-sublattice orbitally ordered state by developing antiferromagnetic orders within each sublattice. States on sublattices $A$ and $B$ form a time-reversal pair and states on sublattices $C$ and $D$ form another time-reversal pair. But, it is not a conventional antiferromagnetic state. In fact, in this phase, the magnetic dipolar moment of the $A$ or $B$ sublattice is nearly perpendicular to the magnetic dipolar moment of the $C$ or $D$ sublattice. Consistent with strong magnetic anisotropy, the staggered magnetizations $\langle \mathbf{j}_A - \mathbf{j}_B + \mathbf{j}_C - \mathbf{j}_D\rangle$ and $\langle \mathbf{j}_A - \mathbf{j}_B - \mathbf{j}_C + \mathbf{j}_D\rangle$ are oriented in a direction very close to the [110] lattice direction.

#### 6. Four-sublattice antiferromagnetic ("$\overline{\Delta}$") state

In the intermediate $J'/J$ and the small $V/J$ regimes, we find another four-sublattice antiferromagnetic phase, the "$\overline{\Delta}$" state. In this regime, the electric quadrupolar interaction may be neglected, and we can understand the state as arising due to the competition between FM and AFM exchange interactions. In the AFM100 phase, every site has 8 NN AFM neighbors and four NN FM neighbors. In the FM111 phase, every site has 0 NN AFM neighbors and 12 NN FM neighbors. In the "$\overline{\Delta}$," we find that, for every site, there are four NN AFM neighbors, which is an intermediate case compared to the FM111 and AFM100 phases. The ground-state wave function of this "$\overline{\Delta}$" phase is parametrized by two complex numbers $x_1$ and $x_2$:

$$|A\rangle = \frac{1}{\sqrt{2}}(x_2|j^z = 2\rangle + \overline{x_2}|j^z = -2\rangle) + x_0|j^z = 0\rangle$$
$$+ \frac{1}{\sqrt{2}}(x_1|j^z = 1\rangle + \overline{x_1}|j^z = -1\rangle), \qquad (65)$$

$$|B\rangle = \frac{1}{\sqrt{2}}(x_2|j^z = 2\rangle + \overline{x_2}|j^z = -2\rangle) + x_0|j^z = 0\rangle$$
$$+ \frac{1}{\sqrt{2}}(-x_1|j^z = 1\rangle - \overline{x_1}|j^z = -1\rangle), \qquad (66)$$

$$|C\rangle = \frac{1}{\sqrt{2}}(\overline{x_2}|j^z = 2\rangle + x_2|j^z = -2\rangle) + x_0|j^z = 0\rangle$$
$$+ \frac{1}{\sqrt{2}}(\overline{x_1}|j^z = 1\rangle + x_1|j^z = -1\rangle), \qquad (67)$$

$$|D\rangle = \frac{1}{\sqrt{2}}(\overline{x_2}|j^z = 2\rangle + x_2|j^z = -2\rangle) + x_0|j^z = 0\rangle$$
$$+ \frac{1}{\sqrt{2}}(-\overline{x_1}|j^z = 1\rangle - x_1|j^z = -1\rangle) \quad (68)$$

with $x_0 = \sqrt{1 - |x_1|^2 - |x_2|^2}$. As one can see from the wave function, states on $A$ and $B$ sublattices form a time-reversal pair and states on $C$ and $D$ sublattices form another time-reversal pair. The magnetic dipolar and quadrupolar orders of each sublattice are found to have the following relation:

$$\langle \mathbf{j}_{A/B} \rangle = \pm m(u_1, u_2, 0), \quad (69)$$

$$\langle \mathbf{j}_{C/D} \rangle = \pm m(u_1, -u_2, 0), \quad (70)$$

$$\langle Q_{A/B/C/D}^{3z^2} \rangle = q, \quad (71)$$

$$\langle Q_{A/B/C/D}^{x^2-y^2} \rangle = q'. \quad (72)$$

Although both "$\Delta$" and "$\overline{\Delta}$" states are four-sublattice states, they are actually different phases. For instance, unlike in the phase "$\Delta$" discussed in the last section, the quadrupole moments in the "$\overline{\Delta}$" phase are uniform. Intuitively, this is because the orbital-orbital interaction is not large enough to induce a two-sublattice structure in this regime.

### 7. Two-sublattice quadrupole (spin nematic) state

With an intermediate $J'/J$ and a large $V/J$, the orbital-orbital interactions dominate over all other interactions in the Hamiltonian. Therefore, the ground state reduces to quadrupolar phase found in Sec. III B. The full set of order parameters is

$$\langle \mathbf{j}_{A/B} \rangle = 0, \quad \langle Q_{A/B}^{3z^2} \rangle = 0, \quad \langle Q_{A/B}^{x^2-y^2} \rangle = \pm q' \quad (73)$$

with $q' = 2\sqrt{3}$.

### 8. $T = 0$ transitions

At the mean-field level, the nature of the transitions between different phases can be understood from the wave functions. If the wave function of one phase can be continuously tuned to that of the neighboring phase, then the phase transition between these two phases may be continuous. Otherwise, it is first order. We find that the possible continuous transitions are FM111-"$*$", "$*$"-FM110, FM110-quadrupolar, quadrupolar-"$\Delta$," and "$\overline{\Delta}$"-AFM100. The remaining transitions are first order at mean-field level. We do not discuss fluctuation effects here, which would be required for a full understanding of the transitions.

## IV. $T > 0$ PHASES

In this section, we study the effects of thermal fluctuations on the phase diagram for $T > 0$. We do this by using standard Weiss mean-field theory, taking into account the symmetry structure of the phases identified in Sec. III. The mean-field method produces self-consistent equations for the order parameters, which can be solved, choosing the solution with minimal free energy, to obtain the temperature dependence of physical quantities. These equations are generally sufficiently complicated that, even taking into account symmetry conditions, only a numerical solution is possible.

Before presenting the numerical solution, we discuss a few aspects of the phase diagram, which can be understood analytically. Specifically, we consider the instabilities of the paramagnetic state on decreasing the temperature from large to small values. Several instabilities are possible, which are signaled in the mean-field calculations by the appearance of a solution of a given symmetry $S$ at a temperature $T_S$. Mathematically, the temperature $T_S$ is defined by the vanishing of the coefficient of the quadratic term in the order parameter associated with the symmetry $S$ in the Landau free energy or, equivalently, the divergence of the mean-field susceptibility of the $S$ order parameter. The order parameters in question are the magnetization vector and quadrupolar tensor at $\mathbf{p} = \mathbf{0}$ and at $\mathbf{p} = \mathbf{Q} = 2\pi(001)$ [note that the four-sublattice states should be described by several $\mathbf{p} = 2\pi(001)$ wave vectors]. In this way, we obtain four temperatures $T_m(\mathbf{0})$, $T_m(\mathbf{Q})$, $T_Q(\mathbf{0})$, $T_Q(\mathbf{Q})$. For a given value of the exchange parameters $(J, J', V)$, the *largest* of these temperatures will determine the actual instability of the paramagnetic state, and thus the first type of order that is encountered upon lowering the temperature. In principle, a first-order transition could also occur at a temperature higher than this, but the full mean-field solution shows that this does not occur except in a region where $J'/J, V/J \ll 1$.

The instability temperatures may be determined analytically. One finds

$$T_m(\mathbf{0}) = \frac{6J' - 2J}{5} + \frac{\sqrt{2J^2 - 20JJ' + 52J'^2}}{5}, \quad (74)$$

$$T_Q(\mathbf{0}) = \frac{7}{60}(J - 6J' + 7V), \quad (75)$$

$$T_m(\mathbf{Q}) = \frac{2}{15}\left[J - 2J' + r\cos\frac{\alpha}{3}\right], \quad (76)$$

$$T_Q(\mathbf{Q}) = \frac{7}{180}(-3J + 18J' + 43V). \quad (77)$$

Here, we defined

$$r = \sqrt{6J^2 - 20JJ' + 32J'^2}, \quad (78)$$

$$\alpha = \text{Arg}[5 - 72y + 204y^2 - 160y^3$$
$$+ i\sqrt{(r/J)^6 - (5 - 72y + 204y^2 - 160y^3)^2}], \quad (79)$$

and $y = J'/J$.

In the parameter space depicted in Fig. 1, $T_Q(\mathbf{p} = \mathbf{0})$ is always smaller than the other three temperatures. Thus, there is never an instability of the paramagnet to a uniform quadrupolar ordered state. Comparing the remaining three temperatures, we find three distinct regions shown in Fig. 2. In region I, the highest transition temperature is $T_m(\mathbf{Q})$, and magnetic order with an enlarged unit cell sets in directly from the paramagnetic state. In region II, the highest transition temperature is $T_Q(\mathbf{Q})$ and two-sublattice quadrupolar (spin nematic) phase occurs neighboring the paramagnetic state. In region III, the highest transition temperature is $T_m(\mathbf{Q})$, and the paramagnetic phase undergoes a transition directly to a ferromagnetic one.

On further lowering of temperature, additional phases may occur. Full mean-field calculations show that there are, in fact,
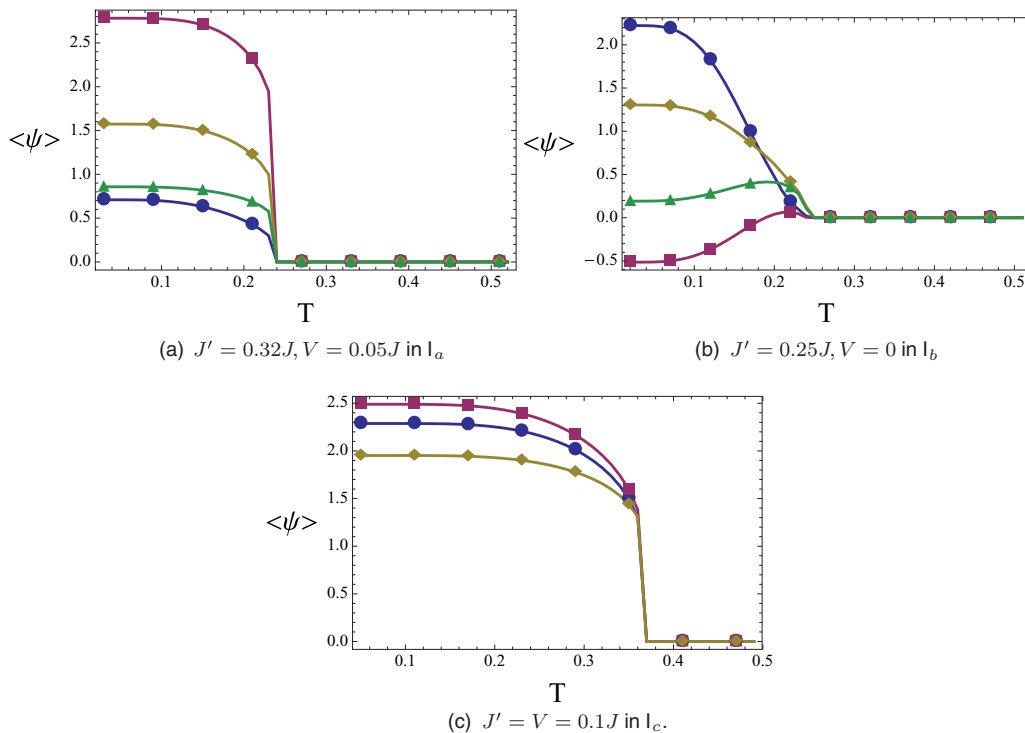
(a) $J' = 0.32J, V = 0.05J$ in $I_a$

(b) $J' = 0.25J, V = 0$ in $I_b$

(c) $J' = V = 0.1J$ in $I_c$.

FIG. 3. (Color online) Order parameters plotted for three subregions of region I: (a) Square (red) $(\langle Q_A^{x^2-y^2} - Q_B^{x^2-y^2}\rangle)/2$, ball (blue) $\langle Q_A^{3z^2} + Q_B^{3z^2}\rangle/2$, diamond (yellow) $|\langle \mathbf{j}_A + \mathbf{j}_B\rangle|/2$, and triangle (green) $|\langle \mathbf{j}_A - \mathbf{j}_B\rangle|/2$. (b) Square (red) $\sum_{i=A,B,C,D}\langle Q_i^{3z^2}\rangle$, ball (blue) $\sum_{i=A,B,C,D}\langle Q_i^{x^2-y^2}\rangle$, diamond (yellow) $|\langle j_A^x - j_B^x + j_C^x - j_D^x\rangle|/4$, and triangle (blue) $|\langle j_A^y - j_B^y - j_C^y + j_D^y\rangle|/4$. (c) Square (red) $\langle Q_A^{x^2-y^2} + Q_B^{x^2-y^2}\rangle/2$, ball (blue) $\langle Q_A^{3z^2} + Q_B^{3z^2}\rangle/2$, and diamond (yellow) $|\langle \mathbf{j}_A - \mathbf{j}_B\rangle|/2$.

10 different patterns of thermal evolution, indicated by the different subregions in Fig. 2. We discuss this in further detail below.

### A. Region I

In region I, the system has a direct transition from the high-temperature paramagnetic phase to low-temperature magnetically ordered phases specified by the dashed curves in Fig. 2. At mean-field level, the transitions to the FM110 phase in region $I_a$ and AFM100 phase in region $I_c$ are found to be first order, while a continuous transition to the four-sublattice "$\overline{\Delta}$" phase is observed in region $I_b$ (see Fig. 3).

### B. Region II

In region II, there is a broad $\mathbf{p} = 2\pi(001)$ quadrupolar phase in the intermediate temperature. Unlike the spin nematic state in the ground-state phase diagram, this intermediate temperature quadrupolar phase is actually a biaxial spin nematic state in which the quadrupole moment $\langle Q_i^{\mu\nu}\rangle$ has three distinct eigenvalues. At mean-field level, the transition from the paramagnetic phase to quadrupolar phase is continuous (see Figs. 4 and 5). Beyond mean-field theory, this transition is believed to be in a three-dimensional $O(3)$ universality class.[9]

As mentioned previously, the low-temperature phases (FM110 in region $II_a$, phase "$\Delta$" in region $II_c$) can be regarded as further breaking the time-reversal symmetry coming from the quadrupolar phase at intermediate temperature. This transition is found to be continuous at mean-field level. The symmetry breaking associated with this transition can be described by several Ising order parameters (uniform and staggered magnetization). This transition may be continuous beyond mean field.[9]

The transition from quadrupolar phase to AFM100 in region $II_d$ is found to be strongly first order in mean-field theory (see Fig. 5). This is easy to understand from a simple symmetry analysis. The AFM100 phase has a uniform orbital configuration and its symmetry is not a subgroup of the quadrupolar phase. Hence, it is almost impossible for the transition to be continuous.

### C. Region III

In region III, the intermediate temperature phase is FM111 (see Fig. 6). The transition from paramagnetic to FM111 is found to be continuous at mean-field level. The transition from FM111 to low-temperature phases (FM110 and phase "$*$") is also found to be continuous in our mean-field analysis. The transition from FM111 to phase FM110 can be simply described by an Ising variable $m^z$. Similarly, the transition from FM111 to phase "$*$" can also be described by an Ising value, which is the staggered magnetization. Thus, these two transitions could be continuous beyond mean field.

### D. Magnetic susceptibility

In this section, we discuss the magnetic response at $T > 0$. We focus particularly on the intriguing nonmagnetic quadrupolar phase of region II in Fig. 2. The magnetic response
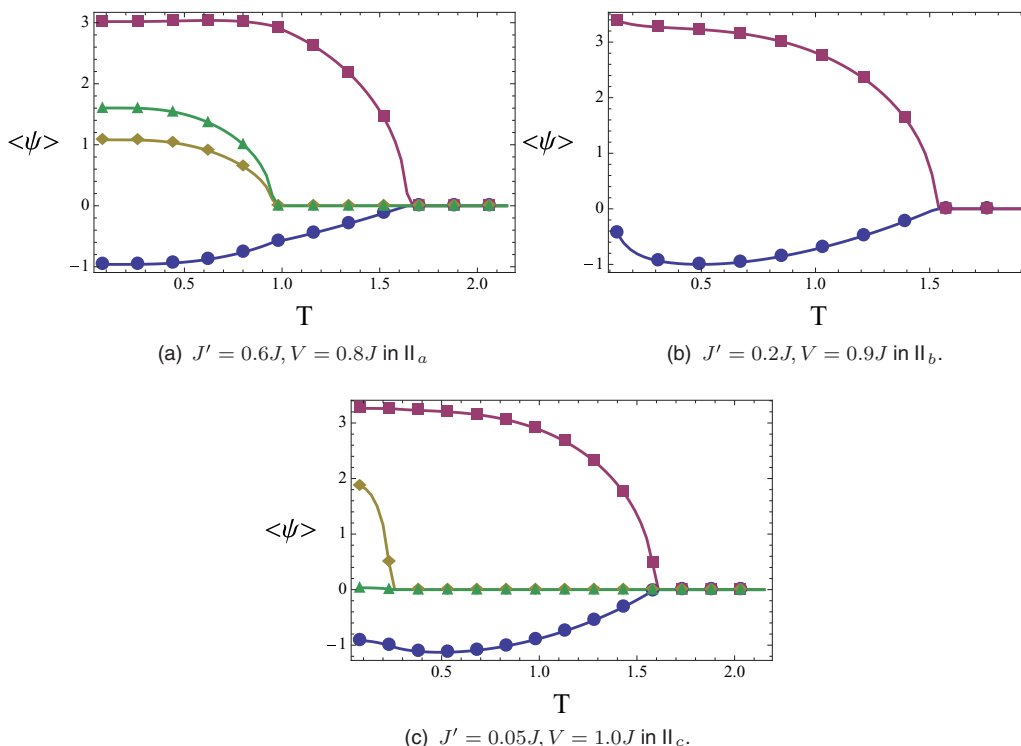
(a) $J' = 0.6J, V = 0.8J$ in $II_a$



(b) $J' = 0.2J, V = 0.9J$ in $II_b$.



(c) $J' = 0.05J, V = 1.0J$ in $II_c$.

FIG. 4. (Color online) Order parameters plotted in four subregions of region II: (a) Square (red) $\langle Q_A^{x^2-y^2} - Q_B^{x^2-y^2}\rangle/2$, ball (blue) $\frac{1}{2}\langle Q_A^{3z^2} + Q_B^{3z^2}\rangle$, triangle (green) $|\langle \mathbf{j}_A + \mathbf{j}_B\rangle|/2$, and diamond (yellow) $|\langle \mathbf{j}_A - \mathbf{j}_B\rangle|/2$. (b) Square (red) $\langle Q_A^{x^2-y^2} - Q_B^{x^2-y^2}\rangle/2$ and ball (blue) $\frac{1}{2}\langle Q_A^{3z^2} + Q_B^{3z^2}\rangle$. (c) Square (red) $\langle Q_A^{x^2-y^2} + Q_B^{x^2-y^2} - Q_C^{x^2-y^2} - Q_D^{x^2-y^2}\rangle/4$, ball (blue) $\sum_{i=A,B,C,D}\langle Q_i^{3z^2}\rangle/4$, and diamond (yellow) $\langle Q_A^{x^2-y^2} + Q_B^{x^2-y^2}\rangle/2$, upper triangle (green) $|\langle \mathbf{j}_A - \mathbf{j}_B\rangle|/2$, and down triangle (blue) $|\langle \mathbf{j}_A + \mathbf{j}_B\rangle|/2$.

is found to be an important indicator for the quadrupolar ordering transition.

The general features, observed in Fig. 7, are as follows. At high temperatures, the magnetic susceptibility $\chi$ obeys the Curie-Weiss law $\chi^{-1} \sim A(T - \Theta_{CW})$, when $T \gg \Theta_{CW}$. The Curie-Weiss temperature is readily obtained from a high-temperature series expansion

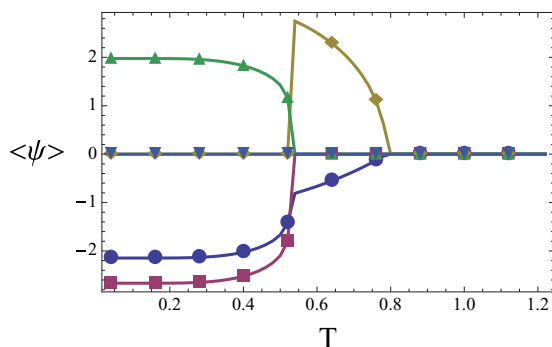$$\Theta_{CW} = \frac{-17J + 66J'}{25}. \tag{80}$$



FIG. 5. (Color online) Order parameters in region $II_d$ with $J' = 0.1J, V = 0.5J$: square (red) $\langle Q_A^{x^2-y^2} - Q_B^{x^2-y^2}\rangle/2$, ball (blue) $\frac{1}{2}\langle Q_A^{3z^2} + Q_B^{3z^2}\rangle$, diamond (yellow) $\langle j_A^y - j_B^y + j_C^y - j_D^y\rangle/4$, and triangle (green) $\langle j_A^y - j_B^y - j_C^y + j_D^y\rangle/4$.

From the mean-field solution, we obtain the susceptibility at lower temperature. At the quadrupolar ordering transition, a cusp in $\chi$ is observed (see Fig. 7). This cusp separates the true Curie-Weiss regime of the paramagnetic phase from a second Curie-Weiss regime at intermediate temperatures. The existence of two Curie-Weiss regimes can be understood as due to the remaining magnetic degeneracy of the quadrupolar phase. Specifically, the intermediate quadrupolar phase partially lifts the fivefold spin-orbital degeneracy, giving rise to a local doublet, which is a time-reversal pair. One should note that this pair is not, however, a Kramer's pair. This doublet is responsible for the Curie-Weiss behavior at the intermediate temperature regime. Looking in more detail, since the spin nematic phase at intermediate temperature has a tetragonal symmetry, we obtain two different susceptibilities: parallel to the wave vector $p = 2\pi(001)$ ($\chi_{zz}$) and normal to it ($\chi_{xx} = \chi_{yy}$). As the temperature is lowered further and magnetic order develops, this is reflected in additional features in the susceptibility.

## V. DISCUSSION

In this paper, we introduced and analyzed a spin-orbital model to describe the localized electrons in a $4d^2$ or $5d^2$ configuration on an fcc lattice, in which strong spin-orbit coupling and the threefold degeneracy of the two-electron orbital states combine to induce a local effective $j = 2$ moment. Nearest-neighbor antiferromagnetic and ferromagnetic exchange interactions and electric quadrupolar interaction
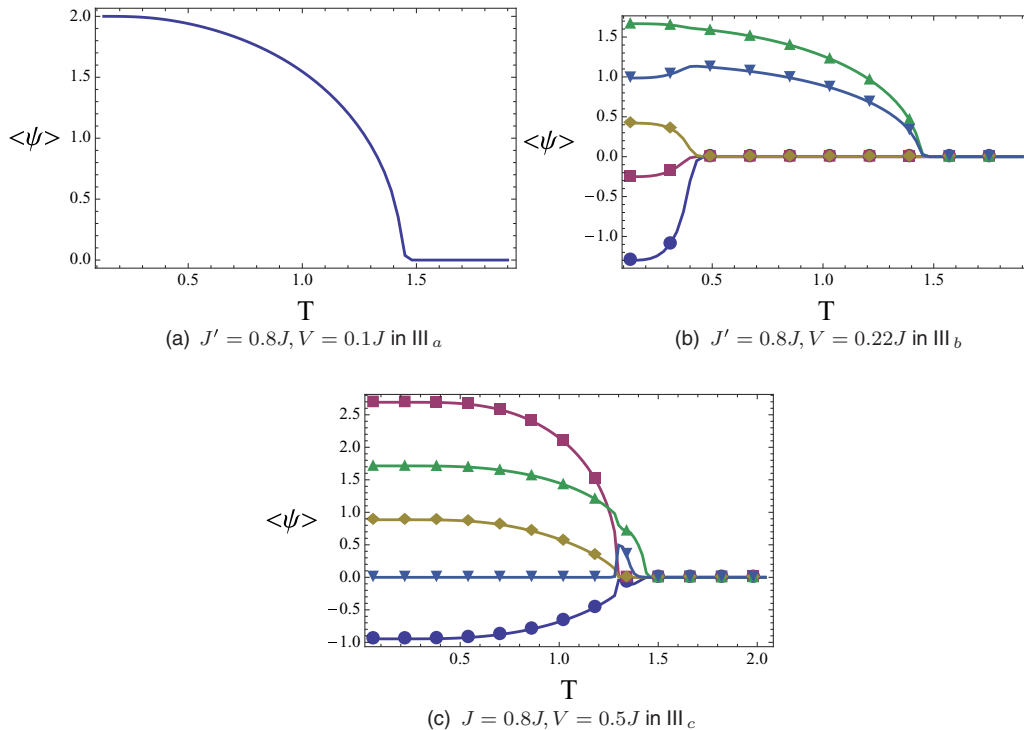
(a) $J' = 0.8J, V = 0.1J$ in III$_a$



(b) $J' = 0.8J, V = 0.22J$ in III$_b$



(c) $J = 0.8J, V = 0.5J$ in III$_c$

FIG. 6. (Color online) Order parameters plotted in three subregions of region III: (a) Uniform magnetization $|\langle \mathbf{j}_i \rangle|$. (b) Square (red) $\langle Q_A^{3z^2} + Q_B^{3z^2} \rangle / 2$, ball (blue) $\langle Q_A^{x^2-y^2} - Q_B^{x^2-y^2} \rangle / 2$, diamond (yellow) $|\langle \mathbf{j}_A - \mathbf{j}_B \rangle / 2|$, upper triangle (green) $|\langle \mathbf{j}_A^\perp + \mathbf{j}_B^\perp \rangle / 2|$, and down triangle (blue) $|\langle \mathbf{j}_A^z + \mathbf{j}_B^z \rangle / 2|$. (c) Square (red) $\langle Q_A^{x^2-y^2} - Q_B^{x^2-y^2} \rangle / 2$, ball (blue) $\langle Q_A^{3z^2} + Q_B^{3z^2} \rangle / 2$, diamond (yellow) $|\langle \mathbf{j}_A - \mathbf{j}_B \rangle / 2|$, upper triangle (green) $|\langle \mathbf{j}_A^\perp + \mathbf{j}_B^\perp \rangle / 2|$, and down triangle (blue) $|\langle \mathbf{j}_A^z + \mathbf{j}_B^z \rangle / 2|$.

were included in the model Hamiltonian. We obtained the ground-state and finite-temperature phase diagrams by Weiss mean-field theory. Seven different ground states (or low-temperature) phases were found. In a large portion of the parameter space, the system develops a two-sublattice structure of orbital configuration, which is driven by the diagonal orbital-orbital interaction. Most interestingly, a nonmagnetic spin nematic ground state occurs in the ground-state phase diagram and extends to a large portion of the phase diagram at finite temperature. Moreover, we find 10 different ways for the system to evolve from the high-temperature paramagnetic phase to the 7 low-temperature phases.

Our theory has provided numerous predictions for experiment. For the magnetic ordered phases that break time-reversal symmetry, neutron scattering, NMR, and/or magnetization measurements can probe the magnetic structure. For the spin nematic phase, similar to the one-electron case discussed in Ref. 9, the magnetic quadrupole order is expected to induce a distortion of the lattice and lower the crystal symmetry. Specifically, the quadrupolar phase corresponds to the tetragonal space group $P4_2/mnm$ (number 136),[9] distinct from the the cubic space group $Fm\bar{3}m$ of the high-temperature phase. If this distortion leads to a measurable effect, high-resolution x-ray scattering should be able to identify the spin nematic order. The low-temperature spin nematic state may also be identified directly from measurements of the orbital state by resonant x-ray scattering or x-ray reflectometry, which could be compared with the theoretical wave functions in Sec. III B.

Now, we discuss the specific materials that have been studied experimentally to date. We start from Ba$_2$CaOsO$_6$.[13]

It retains the cubic $Fm\bar{3}m$ structure down to 17 K. The Curie-Weiss temperature of this material is $-157$ K. The magnetic moment $1.61\mu_B$ is much smaller than the spin-only contribution $2.83\mu_B$ for spin $S = 1$, but close to our prediction $1.25\mu_B$ based on strong SOC in Sec. II A. The deviation can be understood from the effect of hybridization of the Os $d$ orbitals with the oxygen $p$ orbitals, which increases the local magnetic moment.[9] Both magnetic susceptibility and specific-heat measurement find a single antiferromagnetic phase transition at $T_N = 51$ K. According to our theory, a single magnetic transition corresponds to region I in Fig. 2. Since the low-temperature phase of Ba$_2$CaOsO$_6$ is antiferromagnetic, then the AFM100 and "$\bar{\Delta}$" phases are consistent with magnetization measurements. The enlarged unit cell and detailed orientation of magnetic moments predicted here for these phases should provide targets for future neutron scattering measurements.

The structure of La$_2$LiReO$_6$ was observed to be monoclinic (space group $P2_1/n$).[18] This material has a Curie-Weiss temperature $-204$ K, indicating a large antiferromagnetic exchange. The magnetic moment is $1.97\mu_B$, the smallest of which suggests the importance of strong SOC. Magnetic susceptibility, neutron diffraction, and $\mu$SR did not find magnetic long-range order down to 2 K, pointing to a possible quantum spin-liquid phase in this material. Since this crystal structure of this material deviates strongly from a cubic one, our predictions based on the cubic structure are not applicable. Instead, some splitting of the $j = 2$ manifold should be taken into account. Because this is a non-Kramers ion, one could imagine a trivial nonmagnetic ground state at the single-ion

(a) $J' = 0.4J, V = 0.5J$ in $\text{II}_a$

(b) $J' = 0.2J, V = 0.55J$ in $\text{II}_b$

(c) $J' = 0.05J, V = 1.0J$ in $\text{II}_c$
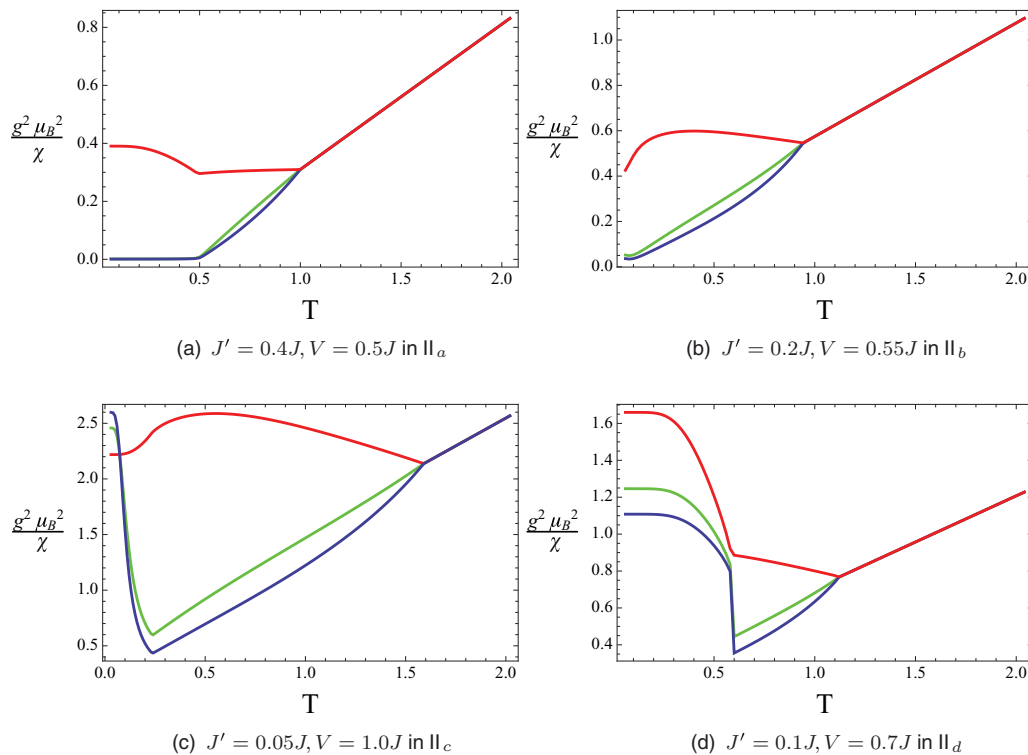
(d) $J' = 0.1J, V = 0.7J$ in $\text{II}_d$

FIG. 7. (Color online) Inverse magnetic susceptibility of different subregions of region II in Fig. 2. Blue (lower) curve: $1/\chi_{xx}$, red (upper) curve: $1/\chi_{zz}$, green (middle) curve: $1/\chi_{\text{powder}}$.

level. However, we note that, in Ref. 18, substantial differences were observed between zero field and field-cooled samples below 50 K, which was argued to be evidence against a single-ion singlet. If the local ground state is instead a doublet, an exotic ground state could be favored, as proposed for the isostructural material $La_2LiMoO_6$.[25] More theoretical and experimental study of the crystal field splitting and multiplet structure is required to further understand the ground state.

$Ba_2YReO_6$ is another material with a cubic crystal structure (space group $Fm\bar{3}m$).[18] The Curie-Weiss temperature is $-616$ K, suggesting a predominant antiferromagnetic exchange. The magnetic moment $1.93\mu_B$ is consistent with the picture of strong SOC. The magnetic susceptibility data clearly suggest two transitions and show two Curie regimes. The first transition is at $\sim 150$ K and the second (spin freezing) transition is at $\sim 50$ K. The second Curie regime appears at the intermediate temperatures between 50 and 150 K. Neutron diffraction shows the absence of detectable magnetic Bragg peaks. $\mu$SR relaxation data observe spin freezing at low temperature. We may speculate that the spin freezing results from disruption by defects of an ordered phase that would otherwise occur in an ideal sample. From the existence of two Curie regimes, we postulate that $Ba_2YReO_6$ corresponds to region II in the phase diagram Fig. 2. This would identify the intermediate temperature phase as a spin nematic. Interestingly, $\mu$SR measured below 100 K found evidence for two spin components, which may be consistent with the two-sublattice nature of the quadrupolar and spin nematic phases. Let us consider the low-temperature phase. Given the very large negative Curie-Weiss temperature, the ferromagnetic exchange is likely

weak in $Ba_2YReO_6$. Hence, comparing with Fig. 1, the natural low-temperature phases are AFM100, the four-sublattice "$\Delta$" phase, or the spin nematic phase. Characterization of the type of disorder in this material would be helpful in further elucidating the physics. It would also be interesting to more directly attempt to detect the proposed quadrupolar order experimentally in the intermediate temperature phase.

This paper (and the related study in Ref. 9) provide a theoretical framework to understand the magnetism and orbital physics of this class of materials. Looking to the future, there is considerable room for refinement of the theory. It would be useful and interesting to include the Jahn-Teller effect, and to develop some microscopic understanding (perhaps from *ab initio* calculations) of the crystal-field splittings in noncubic materials. Within the present model, more studies of thermal and quantum fluctuations beyond mean-field and spin-wave approaches would be desirable. An understanding of the types of disorder in these materials and their effects on the magnetism is also needed. Hopefully, continued pursuit and refinement of measurements on this interesting class of materials will motivate further theoretical work on these and other points.

[1] G. Chen and L. Balents, Phys. Rev. B **78**, 094403 (2008).

[2] B. J. Kim, H. Ohsumi, T. Komesu, S. Sakai, T. Morita, H. Takagi, and T. Arima, Science **323**, 1329 (2009).

[3] M. J. Lawler, A. Paramekanti, Y. B. Kim, and L. Balents, Phys. Rev. Lett. **101**, 197202 (2008).

[4] D. Pesin and L. Balents, Nat. Phys. **6**, 376 (2010).

[5] Y. Okamoto, M. Nohara, H. Aruga-Katori, and H. Takagi, Phys. Rev. Lett. **99**, 137207 (2007).

[6] K. Matsuhira, M. Wakeshima, R. Nakanishi, T. Yamada, A. Nakamura, W. Kawano, S. Takagi, and Y. Hinatsu, J. Phys. Soc. Jpn. **76**, 043706 (2007).

[7] H. Fukazawa and Y. Maeno, J. Phys. Soc. Jpn. **71**, 2578 (2002).

[8] S. Nakatsuji, Y. Machida, Y. Maeno, T. Tayama, T. Sakakibara, J. van Duijn, L. Balicas, J. N. Millican, R. T. Macaluso, and J. Y. Chan, Phys. Rev. Lett. **96**, 087204 (2006).

[9] G. Chen, R. Pereira, and L. Balents, Phys. Rev. B **82**, 174440 (2010).

[10] K. E. Stitzer, M. D. Smith, and H.-C. zur Loye, Solid State Sci. **4**, 311 (2002).

[11] C. Wiebe, J. E. Greedan, G. M. Luke, and J. S. Gardner, Phys. Rev. B **65**, 144413 (2002).

[12] C. R. Wiebe, J. E. Greedan, P. P. Kyriakou, G. M. Luke, J. S. Gardner, A. Fukaya, I. M. Gat-Malureanu, P. L. Russo, A. T. Savici, and Y. J. Uemura, Phys. Rev. B **68**, 134410 (2003).

[13] K. Yamamura, M. Wakeshima, and Y. Hinatsu, J. Solid State Chem. **179**, 605 (2006).

[14] M. A. de Vries, A. C. Mclaughlin, and J.-W. G. Bos, Phys. Rev. Lett. **104**, 177202 (2010).

[15] T. Aharen, J. E. Greedan, C. A. Bridges, A. A. Aczel, J. Rodriguez, G. MacDougall, G. M. Luke, T. Imai, V. K. Michaelis, S. Kroeker, H. Zhou, C. R. Wiebe, and L. M. D. Cranswick, Phys. Rev. B **81**, 224409 (2010).

[16] A. S. Erickson, S. Misra, G. J. Miller, R. R. Gupta, Z. Schlesinger, W. A. Harrison, J. M. Kim, and I. R. Fisher, Phys. Rev. Lett. **99**, 016404 (2007).

[17] T. Aharen, J. E. Greedan, F. Ning, T. Imai, V. Michaelis, S. Kroeker, H. Zhou, C. R. Wiebe, and L. M. D. Cranswick, Phys. Rev. B **80**, 134423 (2009).

[18] T. Aharen, J. E. Greedan, C. A. Bridges, A. A. Aczel, J. Rodriguez, G. MacDougall, G. M. Luke, V. K. Michaelis, S. Kroeker, C. R. Wiebe, H. Zhou, and L. M. D. Cranswick, Phys. Rev. B **81**, 064436 (2010).

[19] E. M. Stoudenmire, S. Trebst, and L. Balents, Phys. Rev. B **79**, 214436 (2009).

[20] A. Läuchli, F. Mila, and K. Penc, Phys. Rev. Lett. **97**, 087205 (2006).

[21] H. Tsunetsugu and M. Arikawa, J. Phys. Soc. Jpn. **75**, 083701 (2006).

[22] D. E. MacLaughlin, Y. Nambu, S. Nakatsuji, R. H. Heffner, L. Shu, O. O. Bernal, and K. Ishida, Phys. Rev. B **78**, 220403 (2008).

[23] S. Bhattacharjee, V. B. Shenoy, and T. Senthil, Phys. Rev. B **74**, 092406 (2006).

[24] S. Nakatsuji, Y. Nambu, H. Tonomura, O. Sakai, S. Jonas, C. Broholm, H. Tsunetsugu, Y. Qiu, and Y. Maeno, Science **309**, 1697 (2005).

[25] T. Todd, T.-P. Choy, and Y. B. Kim, e-print arXiv:1011.6389v1 [cond-mat.str.el] (unpublished).